ORIGINAL PAPER

physica status solidi pss a

www.pss-a.cor

Vertical β-Ga_2O_3 Schottky Barrier Diodes with Enhanced Breakdown Voltage and High Switching Performance

Xing Lu, Xu Zhang, Huaxing Jiang, Xinbo Zou, Kei May Lau, and Gang Wang*

Herein, vertical Schottky barrier diodes (SBDs) based on a bulk β-Ga_2O_3 substrate are developed. The devices feature an ion-implanted planar edge termination (ET) structure, which can effectively smoothen the electric field peak and reduce the electric field crowding at the Schottky junction edge. Greatly enhanced reverse blocking characteristics including $\approx 10^3\times$ lower reverse leakage current and $1.5\times$ higher breakdown voltage (V_B) are achieved, whereas good forward conduction such as a reasonably high on-state current density and near-unity ideality factor is maintained. In addition, the switching performance of the fabricated vertical β-Ga_2O_3 SBDs is investigated using a double-pulse test circuit. When switching from an on-state current of 350 mA to a reverse-blocking voltage of -100 V, the vertical β-Ga_2O_3 SBDs exhibit fast reverse recovery with a reverse recovery time (t_{rr}) of ≈ 14.1 ns and reverse recovery charge (Q_{rr}) of ≈ 0.34 nC, outperforming the Si fast recovery diode (FRD) of similar ratings. The results indicate a great promise of vertical β-Ga_2O_3 SBDs for high-voltage fast switching applications.

1. Introduction

Gallium oxide (Ga_2O_3) semiconductors have emerged as a promising material platform for power electronics, owing to superior material properties such as an ultrawide bandgap of ≈ 4.8 eV and a high breakdown electric field of up to 8 MV cm^{-1}.[1,2] The breakdown electric field of Ga_2O_3 is more than double that of SiC and GaN, which translates to a far superior power device performance predicted by the Baliga's figure-of-merit (BFoM) for unipolar devices.[3,4] In addition, the recent availability of high-quality single-crystalline β-Ga_2O_3 substrates using cost-competitive melt growth methods[5–7] enables the development of vertical β-Ga_2O_3 power devices, which can possess large breakdown voltage with a small footprint, good current handling capability, and high packaging convenience.

Schottky barrier diodes (SBD), featuring low forward voltage drop and fast reverse recovery, are regarded as one of the most important and widely used rectifying and switching devices. To prevent the early onset of impact ionization and premature breakdown of an SBD, the edge termination (ET) technique is typically used to minimize the electric field crowding at the Schottky junction edge. Recently, β-Ga_2O_3-based vertical SBDs have been successfully demonstrated using (010)-, (100)-, ($\bar{2}$01)-, and (001)-oriented bulk β-Ga_2O_3 substrates.[8–14] However, because of the great difficulty of doping Ga_2O_3 into p-type,[15,16] the p–n junction-based ET schemes that are commonly adopted in commercialized Si and SiC power devices are not applicable for Ga_2O_3 power devices. Recently, field plate[17] and trench metal-oxide-semiconductor (MOS) structures[18,19] have been implemented for β-Ga_2O_3-based SBDs to improve their voltage-blocking capabilities by manipulating the electric field distribution at the Schottky junction edge. It was also reported that ion implantation in the device periphery to form a high-resistivity region could be an effective ET method for improving breakdown in both GaN and SiC power diodes.[20,21] In addition to the voltage-blocking capability, the switching performance for a power diode is of fundamental importance, especially in high-efficiency fast switching applications.[22]

In this work, vertical β-Ga_2O_3 SBDs featuring an ion-implanted planar ET are developed on a bulk β-Ga_2O_3 (001) substrate. The high-resistivity region is formed in the SBD periphery by creating nonconductive defects via Ar implantation in the n^--β-Ga_2O_3 drift layer. The device with the Ar-implanted ET shows markedly improved performance when compared with the unterminated one, including $\approx 10^3\times$ reverse leakage reduction and enhanced breakdown voltage (V_B) from 257 to 391 V. Furthermore, the reverse recovery characteristics of β-Ga_2O_3-based SBDs are investigated. A comparison between the β-Ga_2O_3 diode and a commercial Si fast recovery diode (FRD) is also made.

2. Experimental Section

Figure 1 shows the cross-sectional schematic of the vertical β-Ga_2O_3 SBD with the implanted ET. The 8 μm-thick Si-doped n^--β-Ga_2O_3 drift layer was grown on a 640 μm-thick (001) bulk

Dr. X. Lu, Dr. G. Wang
State Key Laboratory of Optoelectronic Materials and Technologies
School of Electronics and Information Technology
Sun Yat-sen University
Guangzhou 510275, China
E-mail: lux86@mail.sysu.edu.cn

Dr. X. Zhang, Dr. H. Jiang, Dr. K. M. Lau
Department of Electronic and Computer Engineering
Hong Kong University of Science and Technology
Kowloon, Hong Kong

Dr. X. Zou
School of Information Science and Technology
ShanghaiTech University
Shanghai 201210, China

The ORCID identification number(s) for the author(s) of this article can be found under https://doi.org/10.1002/pssa.201900497.

DOI: 10.1002/pssa.201900497

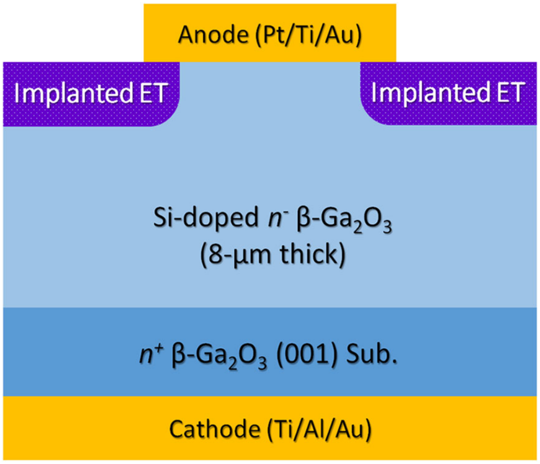

Figure 1. Schematic cross section of the vertical β-Ga_2O_3 SBD with implanted ET fabricated on a bulk substrate.

β-Ga_2O_3 substrate by halide vapor phase epitaxy (HVPE). The substrate was n-type with a Sn doping concentration of $\approx 2.6 \times 10^{18}\,\text{cm}^{-3}$. The net doping concentration ($N_D - N_A$) in the n^--β-Ga_2O_3 drift layer is $\approx 4 \times 10^{16}\,\text{cm}^{-3}$ (in **Figure 2**), as extracted from the capacitance–voltage (C–V) measurement according to

$$N_D - N_A = -\frac{2}{q\varepsilon_s d(1/C^2)/dV} \tag{1}$$

where N_D, N_A, q, and ε_s are donor and acceptor concentrations in the n^--β-Ga_2O_3 drift layer, the electron charge, and the permittivity of β-Ga_2O_3, respectively.

Prior to device fabrication, the sample was cleaned with acetone and isopropanol, followed by a four-cycle deionized (DI) water rinse. After cleaning, a layer of 300 nm SiO_2 was deposited on the sample by plasma-enhanced chemical vapor deposition (PECVD) and patterned, serving as the ion-implantation hard mask. Then, the sample was subjected to a multiple-energy Ar implantation to form the high-resistivity ET structure around the device periphery. High-dose Ar implantation is expected to create defects in β-Ga_2O_3, some of which would locate near the midgap and serve as deep-level traps in β-Ga_2O_3. The energies used in this study were 30, 40, 60, and 80 keV to ensure a high-resistivity region depth of >100 nm, whereas the dose was $1 \times 10^{14}\,\text{cm}^{-2}$ for each energy level. According to a stopping and range of ions in matter (SRIM) simulation, the Ar concentration was over $10^{18}\,\text{cm}^{-3}$ and sufficient to compensate n^--Ga_2O_3 with a carrier concentration of $\approx 4 \times 10^{16}\,\text{cm}^{-3}$. After removal of the SiO_2 hard mask, anode Schottky electrodes were formed by e-beam evaporation of a Pt/Ti/Au (20/100/100 nm) metal stack and a lift-off process. The Schottky metal has a diameter of 100 μm with a 5 μm overlap with the implanted ET region. Finally, a nonalloyed Ti/Al/Au (50/150/200 nm) metal stack was deposited by e-beam evaporation to realize ohmic contact to the backside of the n^+-β-Ga_2O_3 substrate. For comparison, SBDs without ET were also fabricated on the same sample by a similar process except for the ion implantation step.

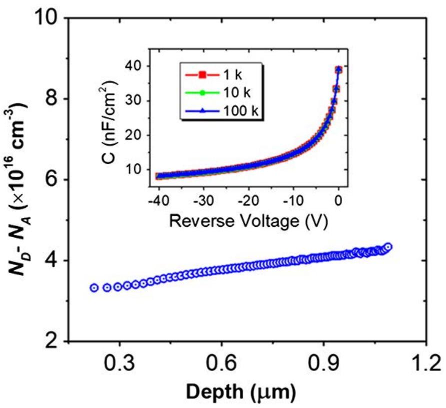

Figure 2. Net doping concentration ($N_D - N_A$) in the n^--β-Ga_2O_3 drift layer extracted from C–V measurement at 100 kHz. Inset: C–V curves measured at different frequencies.

To evaluate the diode's switching performance, a double-pulse test circuit using an inductive load,[22] as shown in **Figure 3**, was implemented. When the metal-oxide-semiconductor field effect transistor (MOSFET) was turned on by the first pulse signal, the inductor (5 mH) was charged linearly by the DC power supply ($V_{DD} = 100$ V) whereas the device under test (DUT) was reverse biased. Once the MOSFET was turned off, the inductor's current went through the DUT and forced it to enter the forward bias condition. When the second pulse occurred, the MOSFET was switched on again and induced the DUT to enter the reverse-blocking state.

3. Results and Discussion

3.1. Static Characteristics

Figure 4a shows the typical forward current–voltage (I–V) curves in linear scale. Both the devices with and without ET showed quite comparable forward I–V characteristics, and a similar specific on-resistance (R_{on}) of $\approx 4\,\text{m}\Omega\,\text{cm}^2$ was extracted at the current density of $\approx 0.3\,\text{kA cm}^{-2}$. The turn-on voltage ($V_{on}$), extracted at the current density of $1\,\text{A cm}^{-2}$, was ≈1.0 V for both the SBDs, in good agreement with the reported results for Pt/β-Ga_2O_3 SBDs in the literature.[1,13,14] The comparable on-state performance indicated that the Ar implantation around the device periphery brought negligible degradation to the Schottky contact.

The semilog plot of the forward I–V curve for the SBD with the implanted EF is shown in Figure 4b. The device exhibited an excellent rectification behavior with a low intrinsic leakage at low bias ($<10^{-10}\,\text{A cm}^{-2}$ below 0.3 V), whereas the on-state current density reached $0.6\,\text{kA cm}^{-2}$ at a forward bias of 4 V,

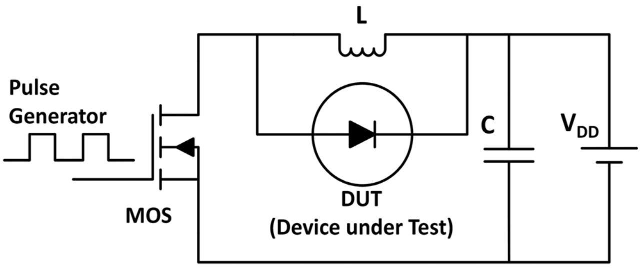

Figure 3. Schematic of double-pulse test circuit.

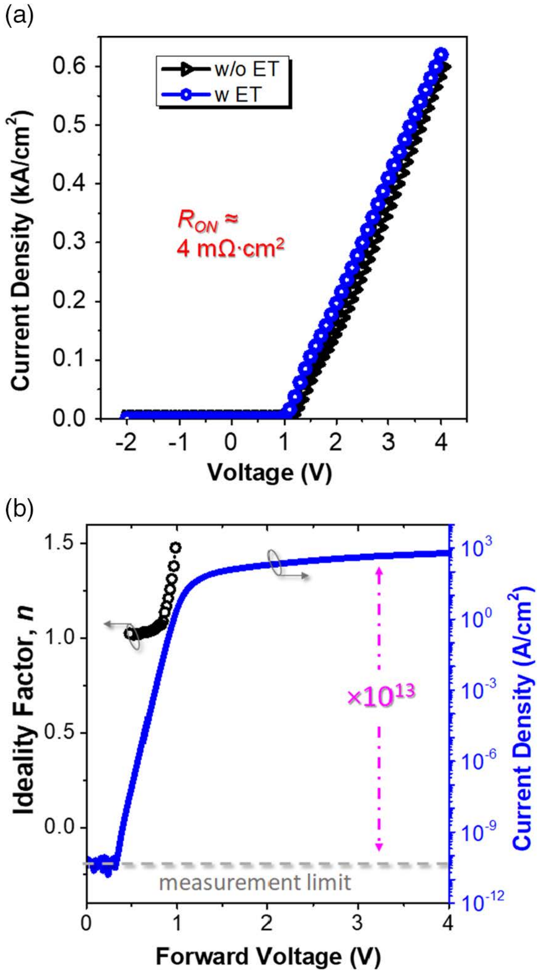

Figure 4. a) Comparison of the forward *I*–*V* characteristics for the fabricated vertical β-Ga_2O_3 SBDs with and without ET in linear scale. b) Forward *I*–*V* curve in the semilog scale and the ideality factor of the SBD with implanted ET.

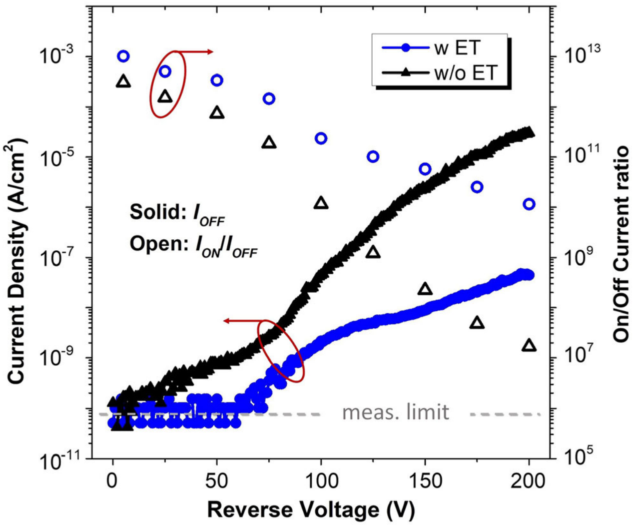

Figure 5. Comparison of the reverse *I*–*V* characteristics and on/off current ratio for the fabricated vertical β-Ga_2O_3 SBDs with and without ET.

leading to a high current swing in the order of 10^{13}. The ideality factor (n) of the Pt/β-Ga_2O_3 SBD was extracted to be 1.02 using the standard thermionic emission mechanisms. It has been reported that trap states at the metal/semiconductor interface and/or defects in the semiconductor bulk could cause increased intrinsic leakage at low bias and nonideality in a SBD. The low intrinsic leakage and near-unity ideality factor in this study indicated a high crystalline quality of the homoepitaxial β-Ga_2O_3 drift layer and good Schottky interface between Pt and β-Ga_2O_3.

Figure 5 compares the reverse *I*–*V* characteristics of the fabricated β-Ga_2O_3 SBDs with and without ET. The typical leakage current density of the SBD without ET is ≈3×10^{-5} A cm^{-2} at a reverse bias of −200 V, whereas the device with the implanted ET exhibited a reverse leakage current density of ≈5×10^{-8} A cm^{-2} at −200 V, ≈3 orders of magnitude lower compared with the unterminated one. The on/off current ratio (I_{ON}/I_{OFF}) for both devices measured at a fixed forward voltage of 4 V and reverse biases from 0 to −200 V is also included in Figure 4. Low reverse leakage current and high I_{ON}/I_{OFF} are critical factors for the realization of high-efficiency power rectifiers. **Figure 6** shows the breakdown characteristics of the vertical β-Ga_2O_3 SBDs with and without ET, where V_B is defined at a reverse leakage current density of 450 μA cm^{-2} with $I_{ON}/I_{OFF} > 10^6$. Compared with the unterminated SBD with V_B of 257 V, the device with the implanted ET yielded an enhanced V_B of 391 V.

Such improvements are attributed to successful ET engineering using Ar implantation. It has been well acknowledged that electrical field crowding occurs at the junction edge of an SBD resulting in low breakdown voltage. In this work, Ar implantation in the SBD periphery creates a high-resistivity region, which promotes the extension of the edge electric field along the surface and results in enhanced V_B. The electric field distributions in the β-Ga_2O_3 SBDs with and without ET were also investigated by a technology computer aided design (TCAD) simulation tool. For simplicity, a single midgap acceptor level with a concentration of 10^{18} cm^{-3} and a depth of 200 nm was

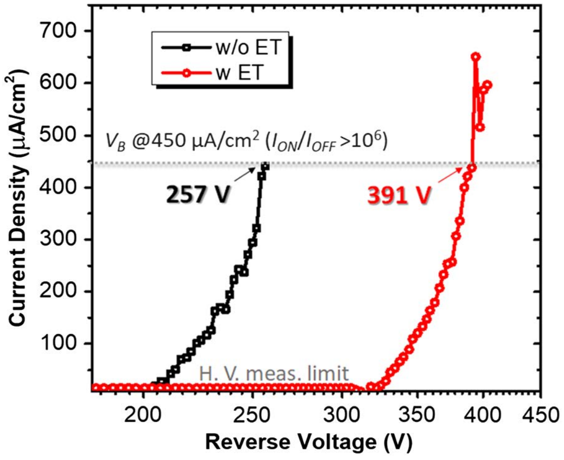

Figure 6. Comparison of the V_B for the fabricated vertical β-Ga_2O_3 SBDs with and without ET. V_B is defined at a reverse leakage current of 450 μA cm^{-2} with $I_{ON}/I_{OFF} > 10^6$.

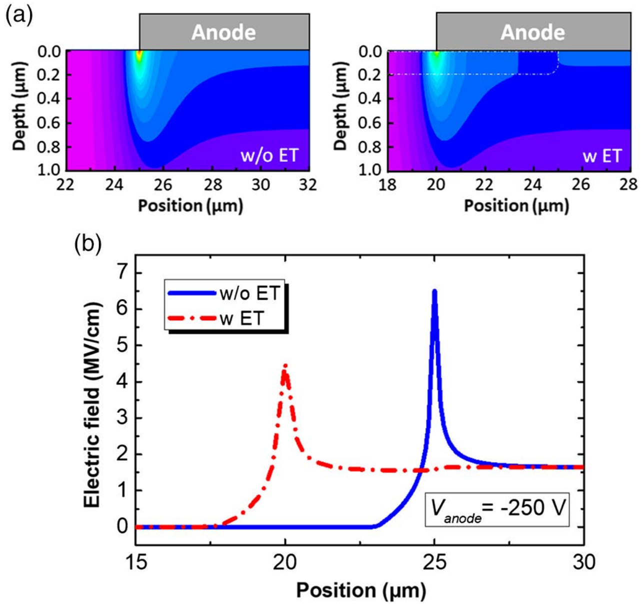

Figure 7. a) A simulated electric field contour map in the vicinity of the anode electrode at a reverse bias of 250 V for the β-Ga_2O_3 SBDs with and without ET. b) Line profile of simulated electric field along the surface of the β-Ga_2O_3 drift layer.

considered for the implantion-induced defects.[23,24] As shown in **Figure 7**, at a reverse bias of 250 V, the simulated peak electric field at the anode electrode edge of the β-Ga_2O_3 SBD was reduced from 6.5 to 4.5 MV cm^{-1} using the implanted high-resistivity ET. On the other hand, the thermal stability of the Ar implantation in β-Ga_2O_3 is a significant issue since the electrical property of the implanted ET may be changed by the annealing effect.[15] After being annealed at 300 °C for 30 min in an atmospheric ambient, no degardation in V_B was observed for the β-Ga_2O_3 SBDs, suggesting a good thermal stability of Ar-implanted ET up to 300 °C.

In addition, for a proper ET, the epitaxial (epi) structure design is of great importance for achieving high performances in a β-Ga_2O_3 SBD. Unfortunately, the combination of doping concentration and thickness of the n^--β-Ga_2O_3 drift layer in this sutdy was yet to be optimized, resulting in a compromised device performance in terms of R_{on} and V_B when compared with the state-of-the-art results in the literature.[14,17,19] Futher improvement could be achieved by optimizing the parameters of the n^--β-Ga_2O_3 drift layer.

3.2. Switching Performance

When a diode is being switched from on-state to off-state, a peak reverse recovery current (I_{rr}) will occur during the removal of the stored charges in the drift region. **Figure 8** shows the reverse recovery characteristics of the β-Ga_2O_3 SBD and Si FRD when switched from a forward current of 350 mA to a reverse-blocking voltage of −100 V with a fixed differential of $dI_F/dt = 10\ A\ \mu s^{-1}$. Compared with the Si FRD (Fairchild, UF4004), the β-Ga_2O_3 SBD exhibited a 12× lower peak reverse recovery current (I_{rr}, ≈38 mA) and a 5.5× reduction in reverse recovery time (t_{rr}, ≈14.1 ns). The reverse recovery charge (Q_{rr}) of the β-Ga_2O_3 SBD is estimated to be 0.34 nC, only around 1.7% of that in the Si FRD. **Table 1** summarises the parameters of the β-Ga_2O_3 SBD and Si FRD during reverse recovery.

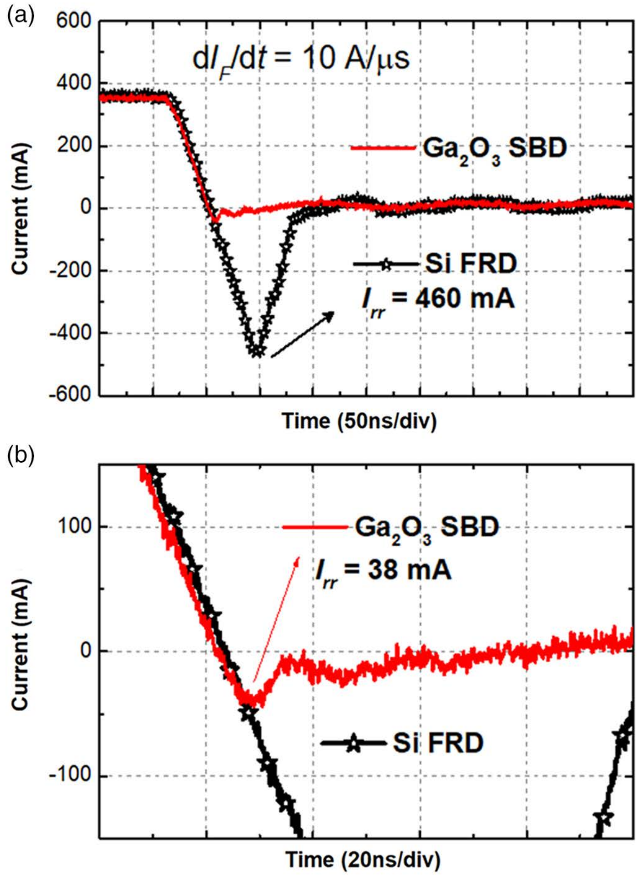

Figure 8. a) Current waveforms of the β-Ga_2O_3 SBD and Si FRD (Fairchild, UF4004) during reverse recovery. b) The zoomed-in image at the point where the β-Ga_2O_3 SBD's peak reverse recovery current occurs.

Compared with the previously reported β-Ga_2O_3 trench MOS SBDs[25] and field-plated SBDs,[26] our device also exhibited competitive switching performance. The reverse recovery charge (Q_{rr}) for all these β-Ga_2O_3 Schottky diodes are quite comparable when taking into account the device size, and the normalized Q_{rr} per device area is around $4 \times 10^{-4}\ C\ cm^{-2}$. Even with similar switching conditions and device sizes,[26] the β-Ga_2O_3 SBDs in our study showed a much smaller peak reverse recovery current (I_{rr}), which chould be attributed to the surpressed reverse leakage current in our device.

Table 1. Summary of the parameters during reverse recovery.

Parameter[a]	β-Ga_2O_3 SBD	Si FRD
I_{rr} (mA)	38	460
t_{rr} (ns)	14.1	77.5
Q_{rr} (nC)	0.34	19.6

[a] Parameters during reverse recovery of β-Ga_2O_3 SBD and Si FRD (Fairchild, UF4004), from a forward current of 350 mA to a reverse-blocking voltage of −100 V.

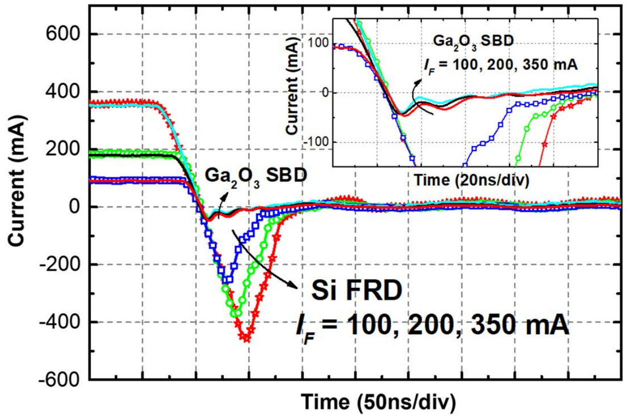

Figure 9. Current waveforms of the β-$\mathrm{Ga_2O_3}$ SBD and Si FRD (Fairchild, UF4004) during reverse recovery from different forward currents. The inset shows the zoomed-in image at the point where the β-$\mathrm{Ga_2O_3}$ SBD's peak reverse recovery current occurs.

Figure 9 shows the reverse recovery characteristics from different forward currents to the same reverse-blocking voltage of -100 V for the β-$\mathrm{Ga_2O_3}$ SBD and Si FRD. For the Si FRD, the larger the forward current, the larger the amount of charges injected into the drift region, prolonging the reverse recovery process, so both I_{rr} and t_{rr} increase significantly as the forward current rises from 100 to 200 and 350 mA. In contrast, less impact was observed for the β-$\mathrm{Ga_2O_3}$ SBD.

4. Conclusions

We developed vertical β-$\mathrm{Ga_2O_3}$ SBDs with an ion-implantation-based planar ET structure and investigated their switching performance. The device with the Ar-implanted ET yielded a $\approx 10^3\times$ lower reverse leakage current when V_B increased from 257 to 391 V, whereas a reasonably high on-state current density and near-unity ideality factor were maintained. Simulations showed that the high-resistivity region created by implantation in the device periphery is highly effective to smoothen the electric field peak at the junction edge. During reverse recovery (switching from an on-state current of 350 mA to a reverse-blocking voltage of -100 V with the differential of $dI_F/dt = 10\ \mathrm{A\ \mu s^{-1}}$), the β-$\mathrm{Ga_2O_3}$ SBD exhibited superior performance to the Si FRD, including a $\approx 12\times$ lower I_{rr}, a $\approx 5.5\times$ lower t_{rr}, and a $\approx 57\times$ lower Q_{rr}. The results suggested a much smaller switching loss and great promise of vertical β-$\mathrm{Ga_2O_3}$ SBDs for high-voltage fast switching applications.

Acknowledgements

This work was supported in part by the International Science and Technology Cooperation Program of Guangzhou under Grant No. 201807010093 and the Frontier and Key Technological Innovation Foundation of Guangdong Province under Grant No. 2017A050506039.

Conflict of Interest

The authors declare no conflict of interest.

Keywords

breakdown voltages, edge termination, reverse recovery, Schottky barrier diodes, β-$\mathrm{Ga_2O_3}$

Received: June 26, 2019
Revised: August 26, 2019

---

[1] M. Higashiwaki, K. Sasaki, A. Kuramata, T. Masui, S. Yamakoshi, *Phys. Status Solidi A* **2014**, *211*, 21.
[2] M. Higashiwaki, G. H. Jessen, *Appl. Phys. Lett.* **2018**, *112*, 060401.
[3] T. P. Chow, I. Omura, M. Higashiwaki, H. Kawarada, V. Pala, *IEEE Trans. Electron Devices* **2017**, *64*, 856.
[4] B. J. Baliga, *IEEE Electron Device Lett.* **1989**, *10*, 455.
[5] E. G. Víllora, K. Shimamura, Y. Yoshikawa, K. Aoki, N. Ichinose, *J. Crystal Growth* **2004**, *270*, 420.
[6] H. Aida, K. Nishigushi, H. Takeda, N. Aota, K. Sunakawa, Y. Yaguchi, *Jpn. J. Appl. Phys.* **2008**, *47*, 8506.
[7] A. Kuramata, K. Koshi, S. Watanabe, Y. Yamaoka, T. Masui, S. Yamakoshi, *Jpn. J. Appl. Phys.* **2016**, *55*, 1202A2.
[8] K. Sasaki, M. Higashiwaki, A. Kuramata, T. Masui, S. Yamakoshi, *IEEE Electron Device Lett.* **2013**, *34*, 493.
[9] Q. He, W. Mu, H. Dong, S. Long, Z. Jia, H. Lv, Q. Liu, M. Tang, X. Tao, M. Liu, *IEEE Electron Device Lett.* **2018**, *39*, 556.
[10] X. Lu, L. Zhou, L. Chen, X. Ouyang, B. Liu, J. Xu, H. Tang, *Appl. Phys. Lett.* **2018**, *112*, 103502.
[11] T. Oishi, Y. Koga, K. Harada, M. Kasu, *Appl. Phys. Exp.* **2015**, *8*, 031101.
[12] J. Yang, S. Ahn, F. Ren, S. J. Pearton, S. Jang, A. Kuramata, *IEEE Electron Device Lett.* **2017**, *38*, 906.
[13] M. Higashiwaki, K. Konishi, K. Sasaki, K. Goto, K. Nomura, Q. T. Thieu, R. Togashi, H. Murakami, Y. Kumagai, B. Monemar, A. Koukitu, A. Kuramata, S. Yamakoshi, *Appl. Phys. Lett.* **2016**, *108*, 133503.
[14] J. Yang, S. Ahn, F. Ren, S. J. Pearton, S. Jang, J. Kim, A. Kuramata, *Appl. Phys. Lett.* **2017**, *110*, 192101.
[15] M. H. Wong, C. Lin, A. Kuramata, S. Yamakoshi, H. Murakami, Y. Kumagai, M. Higashiwaki, *Appl. Phys. Lett.* **2018**, *113*, 102103.
[16] M. H. Wong, K. Goto, H. Murakami, Y. Kumagai, M. Higashiwaki, *IEEE Electron Device Lett.* **2019**, *40*,, 431.
[17] K. Konishi, K. Goto, H. Murakami, Y. Kumagai, A. Kuramata, S. Yamakoshi, M. Higashiwaki, *Appl. Phys. Lett.* **2017**, *110*, 103506.
[18] K. Sasaki, D. Wakimoto, Q. T. Thieu, Y. Koishikawa, A. Kuramata, M. Higashiwaki, S. Yamakoshi, *IEEE Electron Device Lett.* **2017**, *38*, 783.
[19] W. Li, Z. Hu, K. Nomoto, Z. Zhang, J. Hsu, Q. Tu Thieu, K. Sasaki, A. Kuramata, D. Jena, H. G. Xing, *Appl. Phys. Lett.* **2018**, *113*, 202101.
[20] A. M. Ozbek, B. J. Baliga, *IEEE Electron Device Lett.* **2011**, *32*, 300.
[21] D. Alok, B. J. Baliga, P. K. McLarty, *IEEE Electron Device Lett.* **1994**, *15*, 394.
[22] X. Zhang, X. Zou, C. W. Tang, K. M. Lau, *Phys. Status Solidi A* **2017**, *214*, 1600817.
[23] J. L. Lyons, *Semicond. Sci. Technol.* **2018**, *33*, 05LT02.
[24] Linpeng Dong, Renxu Jia, Chong Li, Bin Xin, Yuming Zhang, *J. Alloys Compd.* **2017**, *712*, 379.
[25] A. Takatsuka, K. Sasaki, D. Wakimoto, Q. T. Yhieu, Y. Koishikawa, J. Arima, J. Hirabayashi, D. Inokuchi, Y. Fukumitsu, A. Kuramata, S. Yamakoshi, in *Proc. of the 76th Device Research Conf.*, IEEE, Santa Barbara, CA, USA **2018**, pp. 1–2.
[26] J. Yang, F. Ren, Y. Chen, Y. Liao, C. Chang, J. Lin, M. J. Tadjer, S. J. Pearton, A. Kuramata, *IEEE J. Electron Devices Soc.* **2019**, *7*, 57.